Title

Stochastic transition in synchronized spiking nanooscillators.

Journal

Proceedings of the National Academy of Sciences of USA, 120(38)

Authors

Salev, Pavel
Torres, Felipe
Navarro, Henry
et al.

Publication Date

2023-09-19

DOI

10.1073/pnas.2303765120

Peer reviewed

PNAS RESEARCH ARTICLE | APPLIED PHYSICAL SCIENCES OPEN ACCESS

Stochastic transition in synchronized spiking nanooscillators

Erbin Qiu[a,b,1], Pavel Salev[c], Felipe Torres[d], Henry Navarro[b], Robert C. Dynes[b,1], and Ivan K. Schuller[b]

Edited by Laura Greene, Florida State University, Tallahassee, FL; received March 14, 2023; accepted July 29, 2023

This work reports that synchronization of Mott material-based nanoscale coupled *spiking* oscillators can be drastically different from that in conventional *harmonic* oscillators. We investigated the synchronization of spiking nanooscillators mediated by thermal interactions due to the close physical proximity of the devices. Controlling the driving voltage enables in-phase 1:1 and 2:1 integer synchronization modes between neighboring oscillators. Transition between these two integer modes occurs through an unusual stochastic synchronization regime instead of the loss of spiking coherence. In the stochastic synchronization regime, random length spiking sequences belonging to the 1:1 and 2:1 integer modes are intermixed. The occurrence of this stochasticity is an important factor that must be taken into account in the design of large-scale spiking networks for hardware-level implementation of novel computational paradigms such as neuromorphic and stochastic computing.

spiking oscillators | thermal coupling | synchronization evolution | stochastic transition | time domain phase coexistence

Significance

Synchronization is a universal phenomenon commonly observed in nature, and it has been extensively studied in *harmonic oscillators*. Synchronization of *spiking oscillators* remains less explored despite the increasing interest in using spiking networks in novel computational approaches, such as neuromorphic computing. Here, we use Mott-material-based spiking nanooscillators as a case study to experimentally investigate the synchronization properties arising from the physical interactions between the devices. We found that the transition between different synchronization modes occurs via a stochastic regime in which the spiking pattern unpredictably alternates between the two integer modes instead of desynchronizing or entering a chaotic oscillation regime. This work highlights the unusual dynamic synchronization properties of *spiking oscillators* in contrast to conventional *harmonic oscillators*.

Synchronization is a universal behavior that is commonly observed in a variety of natural and engineered systems (1). In natural systems, synchronization ranges from collective oscillations in bacteria (2) to beating of cilia (3), from rhythms in biological neurons (4, 5) to phase synchronization in the brain (6, 7). Synchronization emerges in engineered physical systems of interacting oscillators, such as nanomechanical and nanoelectromechanical oscillators (8–11), spin Hall and spin torque nano-oscillators (12–15), chemical oscillators (16–18), etc.

With the recent advent of biologically inspired computing, synchronization between special type of oscillators that produce short-duration spikes (in contrast to smoothly evolving harmonic oscillators) has attracted significant attentions (19–21). Spiking oscillators can emulate the electrical activity of brain (22, 23) and can find applications in the development of hardware-level energy-efficient implementations of neural networks (24–26). Recently, we showed that increasing the coupling strength between the antiphase synchronized spiking oscillators leads to synchronization disruptions (21), contradicting naive expectations based on the typical behavior of harmonic oscillators in which stronger coupling develops more robust synchronization. The stark differences between the spiking and harmonic oscillators motivate extensive studies of synchronization phenomena in spiking devices driven by different types of interactions.

This work presents an investigation of the synchronization evolution in coupled spiking nanooscillators based on a Mott material where strong thermal interactions promote in-phase synchronization. We observed the occurrence of unique spiking patterns controlled by a DC voltage applied independently to each oscillator. For small or large applied voltages, the oscillators develop robust 2:1 or 1:1 integer synchronization spiking modes. However, in a relatively wide range of intermediate applied voltages, the oscillators enter a stochastic synchronization regime where the spiking pattern unpredictably alternates between the two discrete integer synchronization modes. These findings highlight unique dynamic synchronization properties of spiking oscillators as compared to conventional harmonic oscillators. The ability to electrically control the synchronization modes and drive the coupled spiking devices into a stochastic synchronization regime is important for practical implementations of neuromorphic and stochastic computing circuits.

We studied spike synchronization in VO_2 nanodevices. VO_2 undergoes an insulator-to-metal transition at T_c = 340 K that can be also triggered by application of an electric stimulus, voltage, or current (27, 28). A 100-nm thick VO_2 thin film was deposited on a (012)-oriented Al_2O_3 substrate by reactive rf magnetron sputtering. Specular x-ray diffraction analysis revealed textured film growth along (110) crystallographic direction (*SI Appendix*, Fig. S1). The film had a sharp insulator-to-metal transition with ~2 orders of magnitude resistance change across T_c (*SI Appendix*, Fig. S2). The film was patterned into 500 × 500 nm^2 devices separated by 500 nm gaps as shown in Fig. 1*A*. The VO_2 between the devices was etched to electrically isolate each device. Although the nanodevices

Author contributions: E.Q., R.C.D., and I.K.S. designed research; E.Q. performed research; E.Q., P.S., F.T., H.N., R.C.D., and I.K.S. contributed new reagents/analytic tools; E.Q., P.S., F.T., H.N., R.C.D., and I.K.S. analyzed data; and E.Q. P.S., and I.K.S. wrote the paper.

The authors declare no competing interest.

This article is a PNAS Direct Submission.

[1]To whom correspondence may be addressed. Email: e3qiu@eng.ucsd.edu or rdynes@ucsd.edu.

This article contains supporting information online at https://www.pnas.org/lookup/suppl/doi:10.1073/pnas.2303765120/-/DCSupplemental.

Published September 11, 2023.

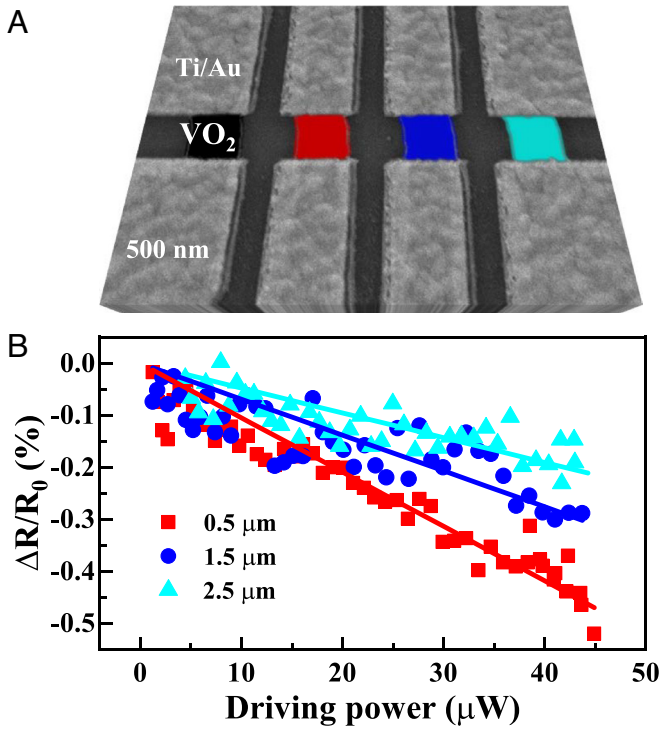

Fig. 1. Heat propagation between nanodevices. (*A*) SEM image with false color of four neighboring VO_2 devices. Each device is 500 × 500 nm^2. The devices are separated by a 500 nm gaps and are electrically isolated from each other. The first device (black) acts as a "heat generator", while the other three (red, blue, and cyan) are "probes". (*B*) Normalized resistance changes ($\Delta R/R_0$) of the second, third, and fourth devices as a function of dissipated power in the first device. The measurements were performed at 327 K base temperature. The resistance decrease with increasing driving power indicates heat propagation from the first device that increases the temperature of the other devices.

are electrically decoupled (Al_2O_3 is a good electrical insulator), they are thermally coupled through the substrate (Al_2O_3 is a good thermal conductor).

Heat propagation is observed by measuring the resistance change ΔR in different nanodevices when one of the neighboring nanodevice is powered with a significant current. This way the powered device acts as a heat generator, while resistance of the surrounding devices serves as probe of the temperature change caused by the heat transfer through the Al_2O_3 substrate. A small 1 μA current was applied to measure the resistance of the probe devices. Such small probing current generates negligible heat and does not induce by itself any noticeable resistance change.

We observed that as the power applied to the heat generator device increases (black device in Fig. 1*A*), the resistances of the neighboring devices decrease linearly (Fig. 1*B*). The resistance of the closest probe device (500 nm distance, red device in Fig. 1*A*) is reduced by ~0.5% at 45 μW power dissipated in the generator device. Comparing this resistance reduction to the equilibrium resistance–temperature dependence (*SI Appendix*, Fig. S2), temperature increase of the closet probe device can be estimated as ~0.1 K. The temperature increase of the probe devices located further away from the generator device, as expected, is smaller, estimated as ~0.06 K at 1,500 nm distance and ~0.03 K at 2,500 nm distance. Detailed resistance–temperature mapping is shown in *SI Appendix*, Fig. S3. The small temperature increase in the probe devices under the employed measurement conditions explains the linear resistance–power dependence in Fig. 1*B*. For higher driving power, the resistance change becomes nonlinear and even displays signatures of the electrical triggering of insulator-to-metal phase transition and filament formation (*SI Appendix*, Fig. S4).

Spiking autooscillations under the application of dc voltage can be produced using a simple circuit shown in Fig. 2*A* (21, 29–31). Individual dc voltage sources power each VO_2 nanodevice. Each nanodevice is connected in series with a load resistor and a 50 Ω input impedance oscilloscope channel to monitor current spikes. At the instant when dc voltage is turned on, voltage over the initially insulating VO_2 nanodevice begins to increase. The voltage increases dynamically, and consequently, the spiking frequency is set by the RC constant of the circuit where the reactive component is due to the parasitic capacitance (estimated as 0.2 nF). When voltage across the nanodevice reaches a threshold, the device transitions into the metallic state which produces a current surge (i.e., a spike) in the circuit. When VO_2 is in the metallic state, most of the applied voltage drops across the load resistor. As only a small voltage is applied across the VO_2, the metallic state cannot be sustained and VO_2 reverts back to the insulating phase. Then, the cycle repeats and persistent generation of spiking autooscillations is established.

Thermal interactions due to the very close physical proximity of the devices promote spike synchronization. When two neighboring oscillators (500 nm separation) are powered individually one at a time with the same voltage of 8.4 V, their inter-spike intervals (ISI) are different, 8.39 μs and 9.89 μs. Overlaying the individually recorded spike current time traces produces an incoherent pattern (Fig. 2*B*). When two neighboring devices are biased with 8.4 V simultaneously, robust in-phase 1:1 current spiking synchronization establishes (Fig. 2*C*), consistent with the previous report (32). We note that resistance between the etched VO_2 nanodevices was higher than the measurement limit (10^{11} Ω) excluding direct electrical current exchange, while capacitive coupling promotes antiphase synchronization (19) inconsistent with our observations. Because we observed thermal interactions in the dc measurements (see Fig. 1*B* and the corresponding discussion), it is reasonable to conclude that the spike synchronization is also driven by thermal interactions. When one device spikes, the heat generated by the current surge propagates to the neighboring device through the sapphire substrate. As the temperature of the neighboring device increases, it approaches the insulator-to-metal transition, which reduces the threshold voltage for the generation of a current spike. Therefore, when one device spikes, it becomes favorable for the neighboring device to spike as well producing the observed 1:1 in-phase synchronization.

When the distance between nanooscillators increases, the thermal coupling between them decreases weakening the synchronization. Application of an above threshold voltage simultaneously to two nanodevices separated by 1,500 nm (first and third devices in Fig. 1*A*) produces unstable synchronization. As shown in *SI Appendix*, Fig. S5, a sequence of several current spikes can be synchronized (i.e., the spikes overlap) while the following spike sequence can be incoherent. At the extreme, two nanodevices at the opposite corners of the sample (~14 mm distance) have completely incoherent current spike sequences when powered simultaneously (*SI Appendix*, Fig. S6). The above observations perfectly follow the expectation for the thermal coupling origin of the synchronization in our spiking nanooscillators.

Varying the driving voltage individually on each nanooscillator leads to the synchronization mode transition as shown in Fig. 3. When the applied voltages are close (for example, 10 V and 9.2 V, Fig. 3*C*), the two devices spike simultaneously, i.e., the synchronization mode is 1:1, similar to the results discussed in the above paragraphs. When one device is powered with a considerably larger voltage than the other one, a different synchronization mode

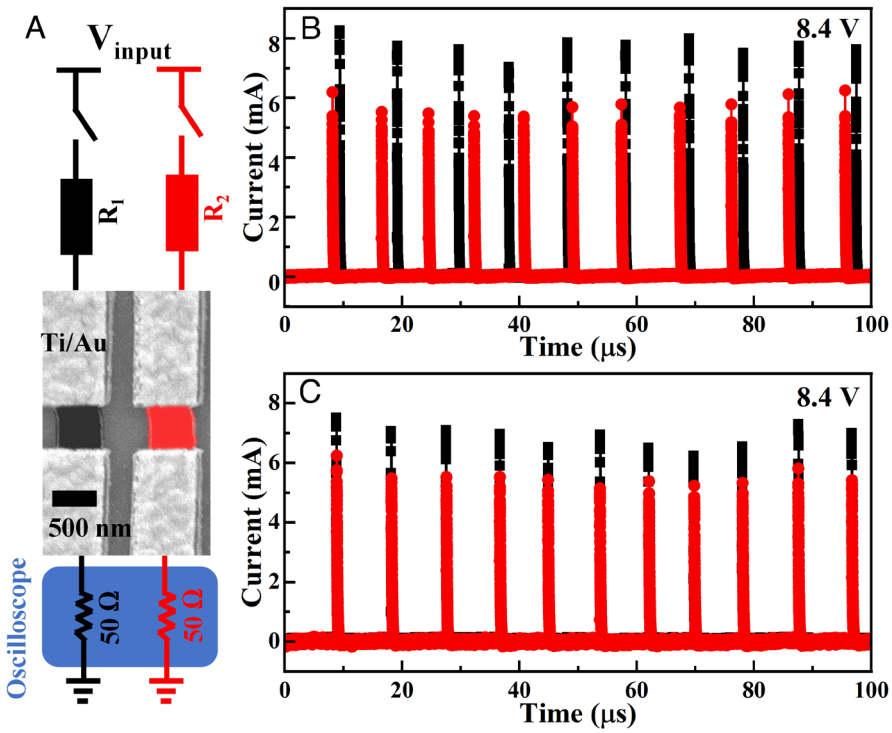

Fig. 2. Synchronization of spiking oscillators via thermal interaction. (*A*) Electrical circuit used to generate spiking oscillations in VO_2 nanodevices. The SEM image shows two neighboring VO_2 nanodevices. (*B*) Overlaid current traces showing incoherent spiking in two *noninteracting* VO_2 nanooscillators when they are biased with 8.4 V independently in two separate measurements. (*C*) Current traces showing coherent in-phase spiking in the same pair of nanooscillators as in *B* when they are biased with 8.4 V simultaneously.

emerges (Fig. 3 *A* and *C*): Every second spike of the high-voltage oscillator coincides with a spike of the low-voltage oscillator, i.e., a 2:1 mode. We note that by fixing voltage on one device and adjusting voltage on the other or vice versa, 2:1 or equivalent 1:2 integer synchronization modes can be established (compare Fig. 3 *A* and *C*), which highlights the generality of this one-to-two spikes synchronization.

One can expect that as the applied voltages changes from the values favoring 2:1 mode to that favoring 1:1 mode, the spikes would first decohere and then lock into the new mode. We found, however, that the transition between the two integer synchronization modes in spiking nanooscillators occurs through an unusual stochastic synchronization regime. Fig. 3 *D* and *E* show that at intermediate applied voltages, the spikes emitted by the two nanodevices are still synchronized, i.e., the spikes always coincide and show no signs of decoherence, but no stable spiking pattern over prolonged time can be discerned. This stochastic synchronization is qualitatively different from the chaotic spiking that has been reported in the MIT-based nanooscillators (33) as the spikes emitted in our devices occur at well-defined time intervals. Instead of chaotic or desynchronized oscillations, the spike sequence in our experiments might show the 1:1 pattern and then unpredictably break with the occurrence of a 2:1 pattern.

It is important to note that the stochastic synchronization found here in closely spaced nanooscillators is in the stark contrast to the behavior in micron-size spiking devices. In the micron-size devices, the transition between 2:1 and 1:1 modes occurs by the development of intermediate noninteger 3:2 and 4:3 modes (32). In our case, the stochastic synchronization between integer modes replaces the transient noninteger modes. We observed the stochastic synchronization in multiple device pairs located in different parts of the VO_2 sample and in multiple samples with different device geometry (*SI Appendix*, Figs. S7 and S8). This robust reproduction of the same phenomenon between different devices and samples suggests that the stochastic synchronization could be a general feature in spiking nanooscillators. Although further studies are necessary to identify critical parameters enabling the stochastic synchronization, it is likely that nanoscale sizes i) make the devices susceptible to fluctuations and ii) allow strong thermal interactions because of the very close proximity as compared to the microscale devices. Our theoretical modeling further supports that the intrinsic stochasticity, i.e., cycle-to-cycle variations of the MIT triggering threshold, and strong thermal coupling promotes stochastic synchronization at the transition between 1:1 and 2:1 modes (*SI Appendix*, Fig. S11), while lowering the thermal coupling strength, e.g., by increasing the separation between the devices, results in noninteger synchronization patterns (*SI Appendix*, Fig. S12).

Synchronization transitions in oscillator systems often display similarities to phase transitions (17). Spatial phase coexistence is the basic feature of the 1st-order phase transition. The stochastic transition between the 2:1 and 1:1 integer synchronization spike sequences in our nanooscillators could be a manifestation of a time domain phase coexistence that develops at the transition between the two integer synchronization modes. Further experimental studies are necessary, however, to test whether the synchronization transition in the coupled spiking oscillators exhibits other features of the 1st-order phase transition, such as hysteretic 2:1 → 1:1 → 2:1 behavior and critical scaling phenomena.

For a quantitative characterization of stochastic synchronization, we analyze the interspike interval (ISI) distribution. Fig. 4*A* shows the ISI time evolution during a 4-ms long measurement (corresponds to several hundred spikes) of one of the nanooscillators during the transition between 2:1 and 1:1 integer synchronization modes. The

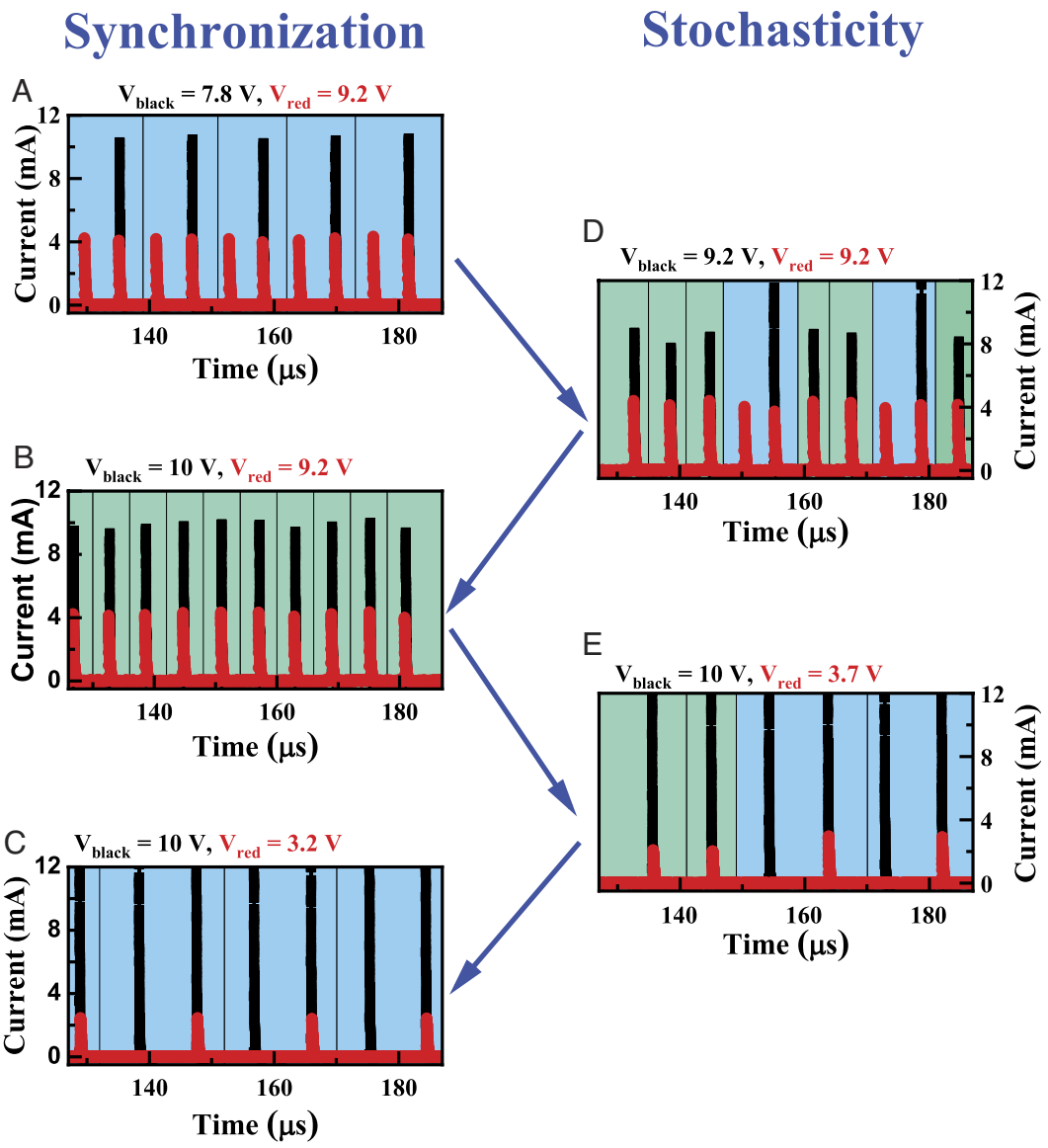

Fig. 3. Synchronized spiking pattern evolution. Current traces displaying spiking oscillations of two VO_2 nanodevices under different applied voltages. (*A*) 2:1 synchronization: two red spikes are locked to one black spike when 9.2 V is applied to the red oscillator and 7.8 V is applied to the black oscillator. (*B*) 1:1 synchronization: each red spike locks into each black spike when 9.2 V is applied to the red oscillator and 10 V to the black oscillator. (*C*) 1:2 synchronization: one red current spike locks into every second black spike when 3.2 V is applied to the red oscillator and 10 V is applied to the black oscillator. (*D* and *E*) Stochastic synchronization emerges at transitions between the modes at intermediate applied voltages. While spikes of the two oscillators overlap, random length spiking sequences corresponding to 2:1 and 1:1 modes (highlighted by green and blue backgrounds, respectively) emerge at random positions.

ISI shows two distinct levels: a larger one of ~18 μs (cyan symbols) that belongs to 2:1 mode, and a smaller one of ~9 μs (blue symbols) that corresponds to 1:1 mode. The ISI spontaneously jumps between the two levels, which is highlighted by light red vertical lines in Fig. 4*A*, providing a visualization of the stochastic synchronization. To obtain the boundaries of the stochastic regime, we sweep the applied voltage of one nanooscillator while keeping the other one at fixed 10 V. By defining the 2:1 mode fraction as

$$\text{2:1 mode fraction} = \frac{\text{Number of ISI of 2:1 mode}}{\text{Total number of ISI}}, \qquad [1]$$

we obtain that the stochastic regime emerges between 3.3 V and 4.2 V as the 2:1 mode fraction changes from 0 to 1 (Fig. 4*B*). By adjusting voltage within the 3.3 to 4.2 V window, it is possible to create spiking sequences that contain random length inclusions of 2:1 mode at random positions, making this stochastic synchronization potentially interesting for stochastic computing and encryption applications (34, 35).

To further evaluate the stochasticity of the spiking sequence transitions, we apply an autocorrelation function (ACF) analysis to the ISI data. To develop sensitivity only to the order of 2:1 mode and 1:1 mode and not to small cycle-to-cycle deviations of the ISI, we converted the ISI data to a binary sequence by defining short ISIs (1:1 mode) as 0's and long ISI's (2:1 mode) as 1's. This conversion can be applied straightforwardly because the ISI data have a clear two-level distribution (Fig. 4*A*). ACF is defined as

$$\text{ACF} = \frac{\sum_{i=1}^{N-k}\left(Y_i - \overline{Y}\right)\left(Y_{i+k} - \overline{Y}\right)}{\sum_{i=1}^{N}\left(Y_i - \overline{Y}\right)^2}. \qquad [2]$$

ACF tests for the presence of repeating patterns in the sequence $\{Y_i\}$ by comparing it to its copy shifted by a time lag k, $\{Y_{i+k}\}$. $\overline{Y}$ in Eq.

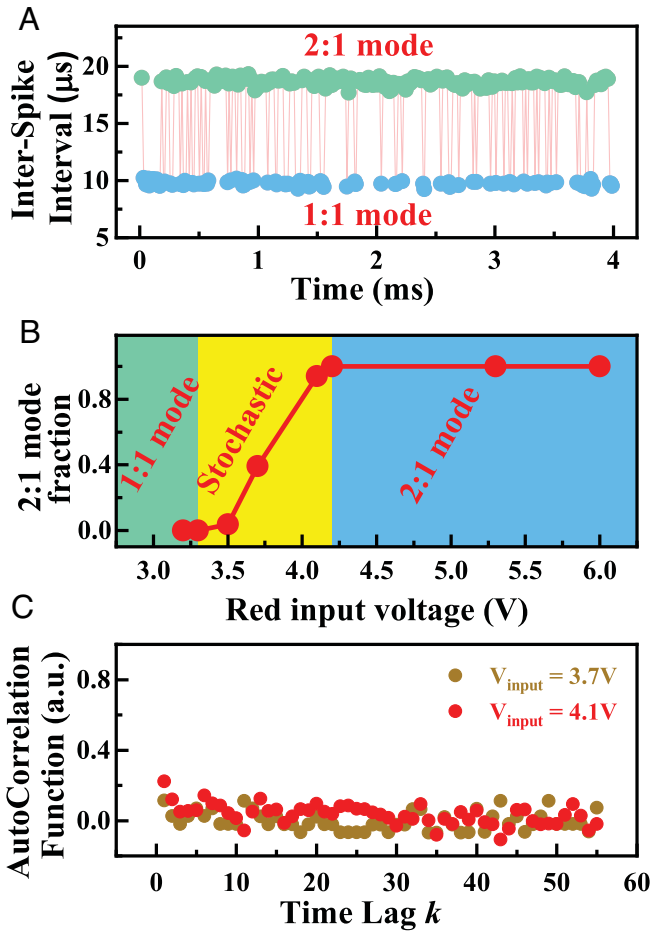

Fig. 4. Stochastic synchronization regime. (*A*) Interspike interval (ISI) evolution of one oscillator at 3.7 V applied voltage when the neighboring oscillator is powered with 10 V at the same time. (*B*) 2:1 mode fraction as a function of applied voltage. The stochastic region appears between 3.3 V to 4.2 V. (*C*) Autocorrelation function (ACF) of two ISI sequences recorded at 3.7 V and 4.1 V. Before applying ACF, the ISI data were converted into binary sequences (see the description in the text).

2 is the mean of the sequence $\{Y_i\}$. ACF is commonly used to test the stochasticity of generated bit sequences (36, 37). As shown in Fig. 3*C*, the ACF of the sequences generated by our nanooscillators at different applied voltages is nearly zero at all time lags, revealing that there is no apparent order in the occurrence of 2:1 mode and 1:1 mode, i.e., the spiking sequence transitions are stochastic.

In summary, we enabled thermally driven synchronization between nanoscale spiking oscillators by placing them in close physical proximity. By controlling the applied voltage, we achieved robust 1:1 and 2:1 synchronization. We found that the transition between the two modes occurs through an extended stochastic synchronization regime where random length spike sequences corresponding to the two modes are intermixed. This stochastic synchronization emerges in nanooscillators instead of noninteger mode that separate different synchronization modes in micron-sized devices (32). In dense integrated circuits containing large number of spiking nanooscillators, for example in neural networks hardware, thermal interactions might become an important factor which determines the circuit operation. Basic understanding of the unique features of spiking nanodevice synchronization, such as the occurrence of the stochastic regime presented in this work, is important for designing circuits capable of harnessing the full potential of novel computational paradigms.

Data, Materials, and Software Availability. All study data are included in the article and/or *SI Appendix*.

ACKNOWLEDGMENTS. This work (E.Q., P.S., F.T., H.N., and I.K.S.) was supported by the Air Force Office of Scientific Research under award number FA9550-22-1-0135. R.C.D. is funded by the Quantum Materials for Energy Efficient Neuromorphic Computing (Q-MEEN-C) Energy Frontier Research Center, funded by the U.S. Department of Energy, Office of Science, Basic Energy Sciences under Award # DE-SC0019273.

Author affiliations: [a]Department of Electrical and Computer Engineering, University of California San Diego, La Jolla, CA 92093; [b]Department of Physics, Center for Advanced Nanoscience, University of California San Diego, La Jolla, CA 92093; [c]Department of Physics and Astronomy, University of Denver, Denver, CO 80208; and [d]Departamento de Física, Facultad de Ciencias, Universidad de Chile, Santiago 7800024, Chile

1. A. Pikovsky, M. Rosenblum, J. Kurths, R. C. Hilborn, Synchronization: A universal concept in nonlinear science. *Am. J. Phys.* **70**, 655–655 (2002).
2. C. Chen, S. Liu, X. Q. Shi, H. Chaté, Y. Wu, Weak synchronization and large-scale collective oscillation in dense bacterial suspensions. *Nature* **542**, 210–214 (2017).
3. Y. Liu, R. Claydon, M. Polin, D. R. Brumley, Transitions in synchronization states of model cilia through basal-connection coupling. *J. R. Soc. Interface* **15**, 20180450 (2018).
4. E. D. Herzog, Neurons and networks in daily rhythms. *Nat. Rev. Neurosci.* **8**, 790–802 (2007).
5. K. M. Hannay, D. B. Forger, V. Booth, Macroscopic models for networks of coupled biological oscillators. *Sci. Adv.* **4**, e1701047 (2018).
6. F. Varela, J. Lachaux, E. Rodriguez, J. Martinerie, The brainweb: Phase synchronization and large-scale integration. *Nat. Rev. Neurosci.* **2**, 229–239 (2001).
7. J. Fell, N. Axmacher, The role of phase synchronization in memory processes. *Nat. Rev. Neurosci.* **12**, 105–118 (2011).
8. M. H. Matheny *et al.*, Exotic states in a simple network of nanoelectromechanical oscillators. *Science* **363**, eaav7932 (2019).
9. S.-B. Shim, M. Imboden, P. Mohanty, Synchronized oscillation in coupled nanomechanical oscillators. *Science* **316**, 95–99 (2007).
10. M. H. Matheny *et al.*, Phase synchronization of two anharmonic nanomechanical oscillators. *Phys. Rev. Lett.* **112**, 014101 (2014).
11. M. C. Cross, A. Zumdieck, R. Lifshitz, J. L. Rogers, Synchronization by nonlinear frequency pulling. *Phys. Rev. Lett.* **93**, 224101 (2004).
12. A. A. Awad *et al.*, Long-range mutual synchronization of spin Hall nano-oscillators. *Nat. Phys.* **13**, 292–299 (2017).
13. R. Lebrun *et al.*, Mutual synchronization of spin torque nano-oscillators through a long-range and tunable electrical coupling scheme. *Nat. Commun.* **8**, 15825 (2017).
14. S. Kaka *et al.*, Mutual phase-locking of microwave spin torque nano-oscillators. *Nature* **437**, 389–392 (2005).
15. A. Houshang *et al.*, Spin-wave-beam driven synchronization of nanocontact spin-torque oscillators. *Nat. Nanotechnol.* **11**, 280–286 (2016).
16. I. Z. Kiss, Y. Zhai, J. L. Hudson, Emerging coherence in a population of chemical oscillators. *Science* **296**, 1676–1678 (2002).
17. D. Călugăru, J. F. Totz, E. A. Martens, H. Engel, First-order synchronization transition in a large population of strongly coupled relaxation oscillators. *Sci. Adv.* **6**, eabb2637 (2020).
18. M. R. Tinsley, S. Nkomo, K. Showalter, Chimera and phase-cluster states in populations of coupled chemical oscillators. *Nat. Phys.* **8**, 662–665 (2012).
19. S. Dutta *et al.*, An Ising Hamiltonian solver based on coupled stochastic phase-transition nano-oscillators. *Nat. Electron.* **4**, 502–512 (2021).
20. S. Dutta *et al.*, Neural sampling machine with stochastic synapse allows brain-like learning and inference. *Nat. Commun.* **13**, 2571 (2022).
21. E. Qiu *et al.*, Stochasticity in the synchronization of strongly coupled spiking oscillators. *Appl. Phys. Lett.* **122**, 094105 (2023).
22. W. Yi *et al.*, Biological plausibility and stochasticity in scalable VO_2 active memristor neurons. *Nat. Commun.* **9**, 4661 (2018).
23. E. M. Izhikevich, Simple model of spiking neurons. *IEEE Trans. Neural Networks* **14**, 1569–1572 (2003).
24. A. Taherkhani *et al.*, A review of learning in biologically plausible spiking neural networks. *Neural Networks* **122**, 253–272 (2020).
25. Q. Duan *et al.*, Spiking neurons with spatiotemporal dynamics and gain modulation for monolithically integrated memristive neural networks. *Nat. Commun.* **11**, 3399 (2020).
26. A. Velichko, V. Putrolaynen, M. Belyaev, Higher-order and long-range synchronization effects for classification and computing in oscillator-based spiking neural networks. *Neural Comput. Appl.* **33**, 3113–3131 (2021).
27. Y. Zhou *et al.*, Voltage-triggered ultrafast phase transition in vanadium dioxide switches. *IEEE Electron Device Lett.* **34**, 220–222 (2013).
28. A. Beaumont, J. Leroy, J. C. Orlianges, A. Crunteanu, Current-induced electrical self-oscillations across out-of-plane threshold switches based on VO_2 layers integrated in crossbars geometry. *J. Appl. Phys.* **115**, 154502 (2014).
29. S. M. Bohaichuk *et al.*, Fast spiking of a mott VO_2–carbon nanotube composite device. *Nano Lett.* **19**, 6751–6755 (2019).
30. T. D. Brown *et al.*, Electro-thermal characterization of dynamical VO_2 memristors via local activity modeling. *Adv. Mater.* **27**, e2205451 (2022).
31. X. Zhang *et al.*, An artificial spiking afferent nerve based on Mott memristors for neurorobotics. *Nat. Commun.* **11**, 51 (2020).

32. A. Velichko, M. Belyaev, V. Putrolaynen, V. Perminov, A. Pergament, Thermal coupling and effect of subharmonic synchronization in a system of two VO_2 based oscillators. *Solid. State. Electron.* **141**, 40–49 (2018).
33. S. Kumar, J. P. Strachan, R. S. Williams, Chaotic dynamics in nanoscale NbO_2 Mott memristors for analogue computing. *Nature* **548**, 318–321 (2017).
34. W. A. Borders *et al.*, Integer factorization using stochastic magnetic tunnel junctions. *Nature* **573**, 390–393 (2019).
35. N. A. Aadit *et al.*, Massively parallel probabilistic computing with sparse Ising machines. *Nat. Electron.* **5**, 460–468 (2022).
36. J. Del Valle *et al.*, Generation of tunable stochastic sequences using the insulator-metal transition. *Nano Lett.* **22**, 1251–1256 (2022).
37. C. Safranski *et al.*, Demonstration of nanosecond operation in stochastic magnetic tunnel junctions. *Nano Lett.* **21**, 2040–2045 (2021).